Analysis and Design of a High-Frequency Low-Profile Converter for Bendable Equipment

Yueshi Guan, *Member, IEEE*, Chang Liu, *Student Member, IEEE*, Yijie Wang, *Senior Member, IEEE*, Wei Wang, and Dianguo Xu, *Fellow, IEEE*

***Abstract*—In this article, a 10-MHz low-profile converter for bendable equipment based on aircore inductor is proposed. The mathematical model and inductance calculation method of the bendable planar circular spiral coil under different bending situations is analyzed. An optimal design method of the T type matching network is depicted in detail which helps to guarantee soft-switching characteristics and high efficiency within the whole bending range by realizing weak inductive equivalent input impedance. A 32 V input, 9V/6.3 W output prototype is proposed in the laboratory and the experimental results verify the feasibility of the proposed optimal design methodology, the system efficiency can be improved by 4% than the traditional method.**

***Index Terms*—Bendable planar coil, high-frequency (HF) converter, matching network, soft-switching characteristics.**

I. Introduction

With the development of material technology, more and more bendable products such as displays, solar cells, and lighting applications gradually appear in the consumer electronics market. Compared with rigid systems, they are light and bendable and more suitable for wearable or portable devices [1]–[3].

To form a bendable system, the power supply of these devices is also expected to own bendable characteristics, among them, much attention has been paid to the bending characteristics of inductors which occupy the largest volume of the power converter. In [4], a boost converter based on the bendable inductance of coaxial cable material is proposed. By increasing the frequency, the energy storage of passive components can be reduced in each switching cycle, and the value of passive components can be reduced. As the frequency increases to tens of megahertz, the power density of the system increases, and planar aircore spiral coils can be used to help reduce the vertical height of the system and form a planar converter [5]–[7].

When these planar structures are considered for bendable power converters, the coil windings can be printed on bendable substrates such as polyimide or polyester film to match the bendability of the system. Square spiral coils are adopted in some bendable power converters including buck, *LLC,* and coupling coils of wireless power transmission systems. The inductance variation of coils at different bending angles is studied by numerical calculation, simulation, and measurement [8]–[13]. However, there is not too much analysis of the plane circular coil which owns a higher quality factor.

It is also worth noting that as the inductance of the planar coil changes under different bending degrees, the system will deviate from the optimal working point. This phenomenon may cause a series of problems such as the loss of soft-switching characteristics, output voltage, and current changes. Although the design in [12]–[15] discussed the influence of bending degrees on the inductance of the coil, no design intervention is made to this influence, and the performance of the system changes drastically under different bending angles.

High frequency (HF) and very HF (VHF) power converters usually consist of three parts: inverter stage, matching network, and rectifier stage. The matching network is a bridge connecting the inverter stage and the rectifier stage to adjust the impedance to improve the power and efficiency of the inverter. For the inverter stage operating at several or tens of MHz frequency level, the Class D topology has the lowest voltage stress and only requires the inductive load to achieve soft switching. When the impedance of matching network is weakly inductive, the body diode of the switch can avoid conducting in the dead zone, thus further reducing the loss of the inverter [16], [17]. Therefore, it is necessary to study how to suppress the influence of the inductance variation on the input impedance angle of the matching network through optimal parameter design. The current research on designing a matching network has always focused on eliminating the impact of load variation. Guan *et al*. [18], [19] designed a pure resistive T-type/π-type matching network for a wide load variation range, and Liu *et al*. [20] designed a π-type matching network to eliminate changes in mutual inductance in wireless power transmission. In [21] and [22], adjustable capacitors are used to design the matching network, and the value of the capacitor is adjusted to ensure that the performance of the system remains unchanged under different loads. The aforementioned existing studies follow the

Manuscript received February 2, 2021; revised April 17, 2021; accepted April 28, 2021. Date of publication May 11, 2021; date of current version July 30, 2021. This work was supported in part by the National Natural Science Foundation of China under Grant 52007041, in part by the Power Electronics Science and Education Development Program of Delta Group under Grant DREG2020008, in part by the Natural Science Foundation of Heilongjiang Province under Grant LH2020E050, and in part by the Youth Talent Project of HIT. Recommended for publication by Associate Editor M. Ponce-Silva. *(Corresponding author: Yueshi Guan.)*

The authors are with the School of Electrical Engineering and Automation, Harbin Institute of Technology, Harbin 150001, China (e-mail: hitguanyueshi @163.com; 18800428682@163.com; wangyijie@hit.edu.cn; wangwei602@hit.edu.cn; xudiang@hit. edu.cn).

Color versions of one or more figures in this article are available at https://doi.org/10.1109/TPEL.2021.3078749.

Digital Object Identifier 10.1109/TPEL.2021.3078749

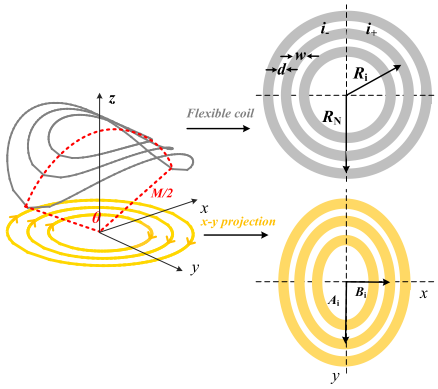

Fig. 1. Bending view of the planar spiral coil.

principle of designing network parameters under the condition of load variation, and the influence of the value deviation of the impedance network itself is rarely mentioned.

In this article, a bendable converter is analyzed based on [23]; Session II analyzes the inductance calculation method of a bendable planar aircore inductor; Session III designs a T-matching network under the condition of bendable inductance. Session IV presents experimental results. Finally, Section V presents the conclusion.

II. Analysis of Bendable Planar Aircore Inductor

The circular spiral coil has an inner diameter of R_1, an outer diameter of R_{N}, and a number of turns of N. The line width is w, the line spacing is d, and the copper thickness is δ. When the coil is bent along the x-axis with an angle θ, the projection of the coil on the xy plane is as shown in Fig. 1.

For the convenience of analysis, as shown in Fig. 1, the coil is divided into two parts along the x-axis. The ith turn conductor in the area where $x>0$ is expressed as i_+, and the ith turn conductor in the area where $x<0$ is expressed as i_-. Then the coordinates of each conductor segment can be expressed as

$$\begin{cases} i_+(x,y,z) \\ =\left[A_i\sqrt{1-\left(\frac{y}{B_i}\right)^2}, y, \sqrt{M^2-y^2}-M\cos\theta/2\right] & y\in[-B_i,B_i] \\ i_-(x,y,z)= \\ \left[A_i\sqrt{1-\left(\frac{y}{B_i}\right)^2}, -y, -\sqrt{M^2-y^2}+M\cos\theta/2\right] & y\in[-B_i,B_i] \end{cases} \tag{1}$$

and among them

$$\begin{cases} M=\frac{2R_N}{\theta} \\ A_i=r_i \\ B_i=\frac{2R_N}{\theta}\sin\frac{r_i\theta}{2R_N}. \end{cases} \tag{2}$$

According to (1), the partial derivative of the coordinates can be obtained as

$$\begin{cases} \frac{\partial i_+(x,y,z)}{\partial y}=\left[\frac{-A_i}{B_i^2}\frac{y}{\sqrt{1-\left(\frac{y}{B_i}\right)^2}}, 1, \frac{-y}{\sqrt{M^2-y^2}}\right] & y\in[-B_i,B_i] \\ \frac{\partial i_-(x,y,z)}{\partial y}=\left[\frac{-A_i}{B_i^2}\frac{y}{\sqrt{1-\left(\frac{y}{B_i}\right)^2}}, -1, \frac{y}{\sqrt{M^2-y^2}}\right] & y\in[-B_i,B_i]. \end{cases} \tag{3}$$

Equation (4) shows the method of calculating the inductance according to Neumann's formula and Rosa's equation [13]

$$L=\begin{cases} \sum_{i=1}^{N}\sum_{j=1}^{N}\frac{\mu}{4\pi}\frac{\vec{dl_i}\cdot\vec{dl_j}}{|l_i-l_j|} & (i\neq j) \\ \sum_{i=1}^{N}\sum_{j=1}^{N}2l_i\left[\log(\frac{2l_i}{\alpha+\beta})+0.5+\frac{0.2235(\alpha+\beta)}{l_i}\right](10^{-6}) & (i=j). \end{cases} \tag{4}$$

Substituting the coordinate vector and partial derivative in (1) and (3) into (4), the mutual inductance between the ith and jth conductors can be deduced as

$$\begin{cases} L(i+,j-)=\frac{\mu}{4\pi}\int_{B_i}^{-B_i}\mathrm{d}y_1\int_{B_j}^{-B_j}f_1(y_1,y_2)\mathrm{d}y_2 \\ L(i+,j+)=\frac{\mu}{4\pi}\int_{B_i}^{-B_i}\mathrm{d}y_1\int_{B_j}^{-B_j}f_2(y_1,y_2)\,\mathrm{d}y_2 \quad (i\neq j) \\ L(i+,j+)=\frac{\mu}{4\pi}\int_{B_i}^{-B_i}\mathrm{d}y_1 \\ \left[\int_{B_j}^{y_1}f_2(y_1,y_2)\mathrm{d}y_2+\int_{y_1}^{-B_j}f_2(y_1,y_2)\mathrm{d}y_2\right] \\ +2\pi r_i\left[\log\left(\frac{2\pi r_i}{w+\delta}\right)+0.5+\frac{0.2235(w+\delta)}{\pi r_i}\right](10)^{-6} \quad (i=j) \end{cases} \tag{5}$$

where the expressions of $f_1(y_1, y_2)$ and $f_2(y_1, y_2)$ are as shown in (6) shown bottom of the next page

Then the self-inductance of the N-turns coils can be solved as follows:

$$L_{coil}=\sum_{i=1}^{N}\sum_{j=1}^{N}[L(i+,j+)+L(i+,j-)]. \tag{7}$$

According to (5), (6), and (7), the inductance calculation program of the circular coil can be designed as the flow chart shown in Fig. 2. In order to speed up the calculation, the coil can be equivalent to multiple linear conductor segments, so that the integral operation in (5) can be replaced by accumulation operation.

According to the above analysis and derivation, the coil inductance under different turns and bending angles is calculated. Since the inductance value is obtained by dividing the circular coil into multiple conductors, as Fig. 2 shows, larger "*Segments*" is recommended under larger coil sizes. The calculated and measured results under different coil dimensions are shown in Fig. 3, which agree well with each other. The error between calculation and measurement of each coil and the selected calculation steps are shown in Table I. All inductances are measured at 10-MHz frequency with Keysight E4990A. When the coil is bent from 0 to 180 degrees, the inductance reduces about 13%. When the coil is bent asymmetrically, the analysis method can also be used, as shown in the Appendix.

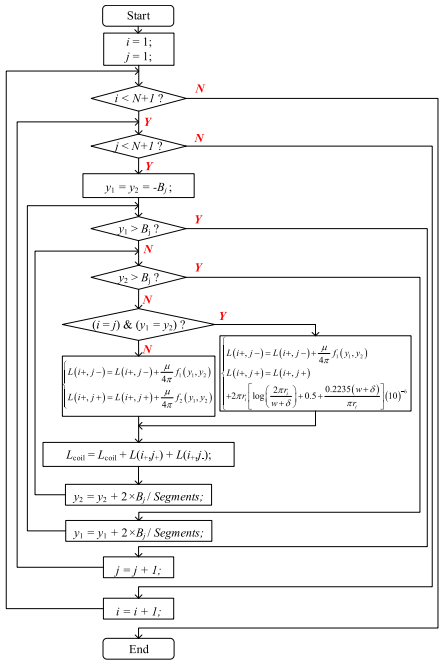

Fig. 2. Flowchart of the calculation process of the bendable coil.

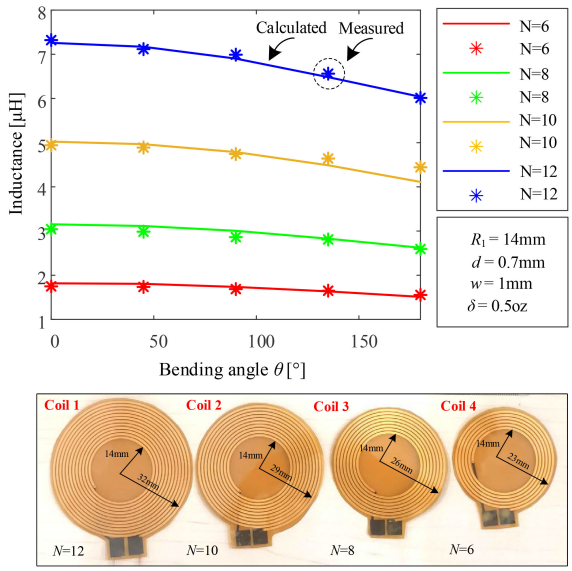

Fig. 3. Relationship between coil bending angle and inductance value.

TABLE I
STEP SIZE AND ERROR OF INDUCTANCE CALCULATION

Turns	*Segments*	$\theta = 0°$	$\theta =$ 45°	$\theta =$ 90°	$\theta =$ 135°	$\theta =$ 180°
N=6	50	3.98%	3.95%	2.91%	0.98%	2.84%
N=8	50	3.68%	4.39%	5.03%	0.61%	1.01%
N=10	80	2.94%	2.84%	2.25%	3.30%	7.43%
N=12	100	4.29%	3.92%	1.37%	1.29%	4.99%

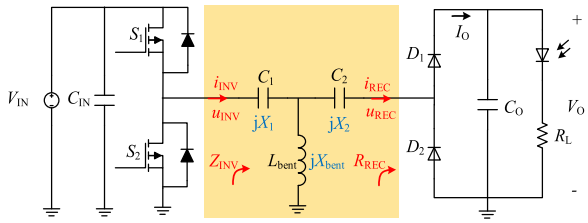

Fig. 4. Circuit diagram of the proposed dc/dc converter.

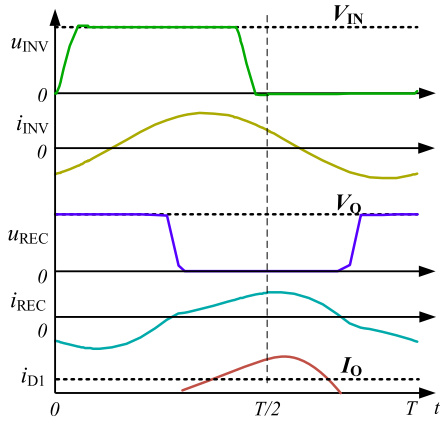

Fig. 5. Voltage and current waveforms of the circuit.

III. ANALYSIS OF THE MATCHING NETWORK

The HF dc/dc converter is usually composed of an inverter, a matching network, and a rectifier. For a bendable dc/dc converter, the most important task is to eliminate the influence of the inductance change on the matching network, which is mainly reflected in the impedance angle. The circuit diagram of the proposed converter and the current and voltage waveforms are shown in Figs. 4 and 5.

u_{REC} and i_{REC} are the output voltage and current of the matching network, u_{INV} and i_{INV} are the input voltage and

$$\begin{cases} f_1(y_1,y_2) = \dfrac{\frac{A_iA_j}{B_iB_j}\frac{y_1y_2}{\sqrt{B_i^2-y_1^2}\cdot\sqrt{B_j^2-y_2^2}} - 1 + \frac{y_1y_2}{\sqrt{M^2-y_1^2}\cdot\sqrt{M^2-y_2^2}}}{\left[\frac{A_iA_j}{B_iB_j}\left(\sqrt{B_i^2-y_1^2}-\sqrt{B_j^2-y_2^2}\right)^2+(y_1-y_2)^2+\left(\sqrt{M^2-y_1^2}-\sqrt{M^2-y_2^2}\right)^2\right]^{\frac{1}{2}}} \\ f_2(y_1,y_2) = \dfrac{\frac{A_iA_j}{B_iB_j}\frac{y_1y_2}{\sqrt{B_i^2-y_1^2}\cdot\sqrt{B_j^2-y_2^2}} + 1 - \frac{y_1y_2}{\sqrt{M^2-y_1^2}\cdot\sqrt{M^2-y_2^2}}}{\left[\frac{A_iA_j}{B_iB_j}\left(\sqrt{B_i^2-y_1^2}-\sqrt{B_j^2-y_2^2}\right)^2+(y_1-y_2)^2+\left(\sqrt{M^2-y_1^2}-\sqrt{M^2-y_2^2}\right)^2\right]^{\frac{1}{2}}}. \end{cases} \tag{6}$$

current, R_{REC} and Z_{INV} are the load and input impedance, respectively. C_1 and C_2 are the resonant capacitors of the matching network.

According to Kirchhoff's voltage and current law and the Fourier transformation, the voltage and current of the matching network can be deduced as

$$\begin{cases} u_{\mathrm{INV}} = i_{\mathrm{INV}} \cdot jX_1 + jX_{\mathrm{coil}} \cdot (i_{\mathrm{INV}} - i_{\mathrm{REC}}) \\ u_{\mathrm{INV}} = i_{\mathrm{INV}} \cdot jX_1 + i_{\mathrm{REC}} \cdot jX_2 + u_{\mathrm{REC}} \\ u_{\mathrm{REC}} = i_{\mathrm{REC}} R_{\mathrm{REC}}. \end{cases} \tag{8}$$

Then the simplified network output to input voltage ratio, the impedance angle and the equivalent impedance R_{REC} of the rectifier can be obtained as

$$\begin{cases} G = \frac{u_{\mathrm{REC}}}{u_{\mathrm{INV}}} = \frac{X_{\mathrm{bent}} R_{\mathrm{REC}}}{(X_1X_2 + X_2X_{\mathrm{bent}} + X_1X_{\mathrm{bent}}) + (X_1 + X_{\mathrm{bent}}) R_{\mathrm{REC}}} \\ \tan \varphi_L \\ = \frac{(X_1X_2 + X_2X_{\mathrm{bent}} + X_1X_{\mathrm{bent}})(X_2 + X_{\mathrm{bent}}) + (X_1 + X_{\mathrm{bent}}) R_{\mathrm{REC}}^2}{X_{\mathrm{bent}}^2 R_{\mathrm{REC}}} \\ R_{\mathrm{REC}} = \frac{4R_L}{\pi^2}. \end{cases} \tag{9}$$

In order to study the design scheme of X_1, X_2, and X_{coil}, intermediate variables m and k are introduced. k is the inductance change ratio which can be expressed as $L_{\mathrm{bent}} = k\, L_{\mathrm{coil}}$, where L_{coil} and X_{coil} are the coil inductance and impedance at $\theta = 0°$, $L_{\mathrm{coil}} = j\omega X_{\mathrm{coil}}$; L_{bent} and X_{bent} are the inductance and impedance at other bending angles, $L_{\mathrm{bent}} = j\omega X_{\mathrm{bent}}$. m is the ratio of X_2 and X_{coil}. Then X_2, X_{bent} can be expressed as

$$\begin{cases} X_2 = -mX_{\mathrm{coil}} \\ X_{\mathrm{bent}} = kX_{\mathrm{coil}}. \end{cases} \tag{10}$$

As analyzed by the earlier section, when the coil is bent to a certain angle, its inductance will decrease accordingly, which leads to a decrease in k. By setting two zero points of the impedance angle φ_{INV} at $k_{\min}$ and $k_{\max}$, φ_{INV} will rise first and then decrease with k, thereby limiting the variation range of φ_{INV}. When the zero point is not set at $k_{\min}$, φ_{INV} will always rise or fall, resulting in a large $\Delta\varphi_{\mathrm{INV}}$.

In addition, the voltage gain of the matching network is $G = u_{\mathrm{INV}}/u_{\mathrm{REC}}$. According to the waveforms in Fig. 5, it can be calculated that $u_{\mathrm{INV}} = 2{*}V_{\mathrm{IN}}/\pi$, $u_{\mathrm{REC}} = 2{*}V_{\mathrm{O}}/\pi$. Then from the above analysis, three constraints of the matching network can be derived as

$$\begin{cases} \varphi_{\mathrm{INV}}|_{k_{\max}} = 0 \\ \varphi_{\mathrm{INV}}|_{k_{\min}} = 0 \\ G|_{k=1} = V_O/V_{\mathrm{IN}}. \end{cases} \tag{11}$$

Actually, the impedance angle should be slightly larger than zero. However, in order to establish the corresponding equation to calculate parameters, the impedance angle is set to zero. When building the prototype, the impedance can be slightly inductive by fine-tuning the inductance and capacitance values.

Substituting (10) into (8) and (9), according to the specified input and output parameters V_{O}, V_{IN}, R_{REC}, and $k_{\min}$, the intermediate variable m can be calculated as

$$m = \frac{\sqrt{[k_{\min}+3+(k_{\min}-3)(V_O/V_{\mathrm{IN}})^2]^2 + 8[k_{\min}-(V_O/V_{\mathrm{IN}})^2+1][(V_O/V_{\mathrm{IN}})^2-1]}}{4} + \frac{k_{\min}+3+(k_{\min}-3)(V_O/V_{\mathrm{IN}})^2}{4}. \tag{12}$$

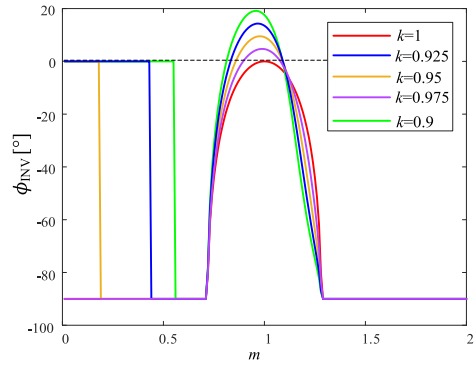

Fig. 6. Change of impedance angle under different m and k. ($V_{\mathrm{o}}/V_{\mathrm{in}} = 0.2813$).

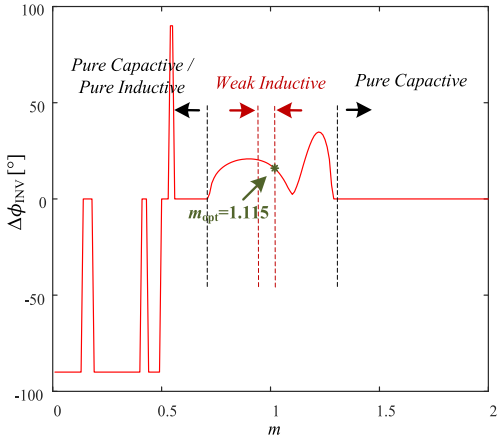

Fig. 7. Relationship between $\Delta\varphi_{\mathrm{INV}}$ and m. ($V_{\mathrm{o}}/V_{\mathrm{in}} = 0.2813$ $k_{\min} = 0.9$).

Taking one situation as an example, Fig. 6 shows the change of φ_{INV} under different values of m, Fig. 7 is the relationship between $\Delta\varphi_{\mathrm{INV}}$ and m based on Fig. 6.

In the next step, X_{coil}, X_2, and X_1 can be obtained from (13) according to m

$$\begin{cases} X_{\mathrm{coil}} = \frac{1}{\sqrt{(V_O/V_{\mathrm{IN}})^2 - (m-1)^2}} R_{\mathrm{REC}} \quad 1 - V_O/V_{\mathrm{IN}} < m < 1 + V_O/V_{\mathrm{IN}} \\ X_2 = \frac{-m}{\sqrt{(V_O/V_{\mathrm{IN}})^2 - (m-1)^2}} R_{\mathrm{REC}} \\ X_1 = \frac{m(1-m) - (V_O/V_{\mathrm{IN}})^2 - (m-1)^2}{(1-m)^2 \sqrt{(V_O/V_{\mathrm{IN}})^2 - (m-1)^2 + [(V_O/V_{\mathrm{IN}})^2 - (m-1)^2]^{1.5}}} R_{\mathrm{REC}}. \end{cases} \tag{13}$$

The specific analysis process can be simplified to the block diagram shown in Fig. 8.

It should be mentioned that the X_1 and X_2 cannot be always capacitive. The capacitive range is in the yellow region as Fig. 9 and (14) show. If $k_{\min}$ and V_{O}, V_{IN} exceed this range, X_1 and X_2 are inductive. For the analysis in this article, X_1 and X_2 just fall into the capacitive, where only one inductor exists in the matching network

$$\begin{cases} k_{\min} < 0.6\,(V_O/V_{\mathrm{IN}}) + 0.7 \quad V_O/V_{\mathrm{IN}} < 0.5 \\ k_{\min} < 1 \qquad\qquad 0.5 < V_O/V_{\mathrm{IN}} < 1.2. \end{cases} \tag{14}$$

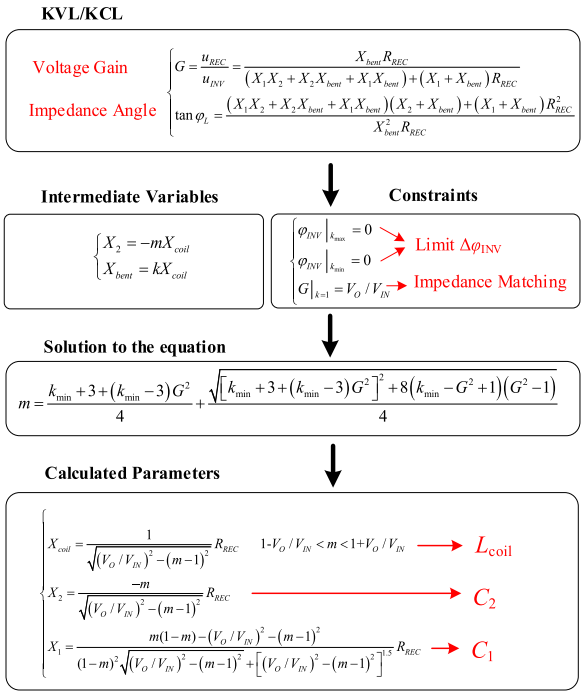

Fig. 8. Flowchart of analysis process of matching network parameters.

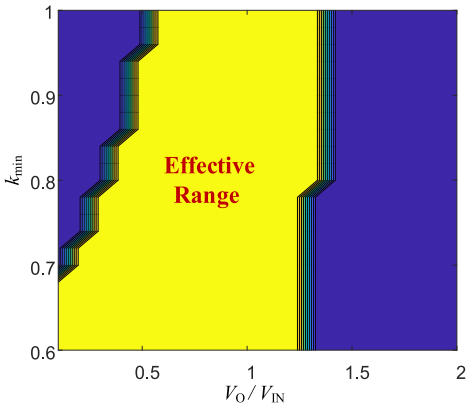

Fig. 9. Effective intervals of X_1 and X_2 are capacitive.

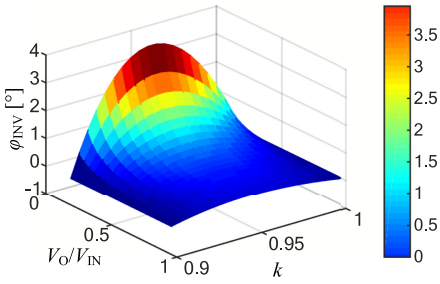

Fig. 10. Relationships between V_O/V_{IN}, k, and φ_{INV} of the proposed matching network.

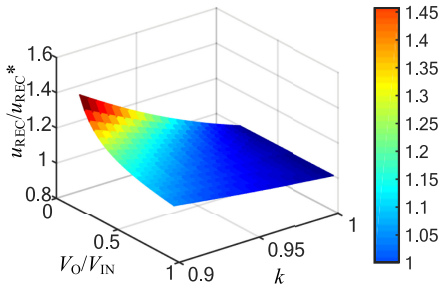

Fig. 11. Relationships between $u_{REC}/u_{REC}*$, k, and V_O/V_{IN} of T-matching network.

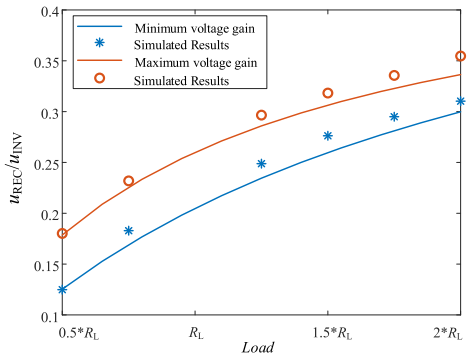

Fig. 12. Performance of the prototype under different loads (rated load R_L = 12.86 Ω, k_{min} = 0.9).

Fig. 10 shows the relationship between V_O/V_{IN}, k, and φ_{INV} of the proposed matching network. It can be seen that the larger the V_O/V_{IN}, the smaller the change in the impedance angle φ_{INV}.

Fig. 11 shows the relationship between the output voltage, voltage transformation ratio V_O/V_{IN}, and inductance change ratio k. $u_{REC}*$ is the rated matching network output voltage, and u_{REC} is the matching network output voltage when the system is bent. It can be seen that as V_O/V_{IN} decreases and k increases, the output voltage gradually shifts from the original value. When V_O/V_{IN} is above 0.5, the output voltage shift rate can be limited to 15%.

Under nonrated loads, the curve of voltage gain of the proposed prototype is shown in Fig. 12. From Fig. 12, as the load increases, the voltage gain of the system continues to increase, which means that when the load changes, the output voltage also changes. Another characteristic is that the voltage range between maximum and minimum remains almost the same.

IV. Experimental Results

A 10 MHz, 9 V/6.3 W with 32 V input voltage prototype is built based on the proposed design method, which helps to verify the feasibility and correctness of the above design method. The specific circuit parameters are shown in Table II. The picture of the prototype is shown in Fig. 13. The load at the back end of the circuit is an OLED panel.

The voltage and current are measured with Agilent DSO7104A, and the power supply for the prototype is RIGOL DP832. Under different coil bending angles, Fig. 14 shows the waveforms of the matching network input voltage u_{INV} and current i_{INV}. Under 0° and 180° bending situations, the resonant

TABLE II
EXPERIMENTAL PARAMETERS OF THE PROTOTYPE

Label	Value	Item
C_1	821pF	700A 821KW (ATC)
C_2	1362pF	700A 681KW (ATC)*2
C_{in}	10uF	GRM21BR61H106KE43L(Murata)
C_o	10uF	GRM21BR61H106KE43L(Murata)
L_{coil}	120nH	R_7=11mm w=1mm d=0.5mm
		N=7 δ=1oz
D_1 , D_2		BAS3010B(Infineon)
S_1 , S_2		EPC2001C(EPC)
Load		LL159FR1(LG)

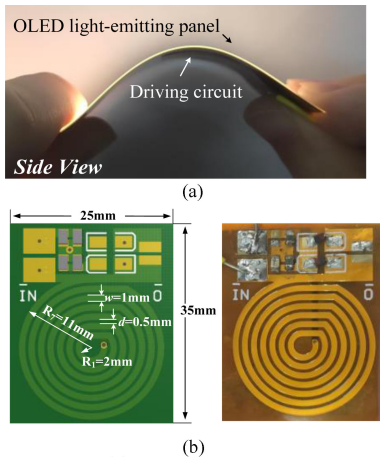

Fig. 13. Prototype of the proposed converter and OLED system. (a) OLED and proposed converter. (b) converter on FPC.

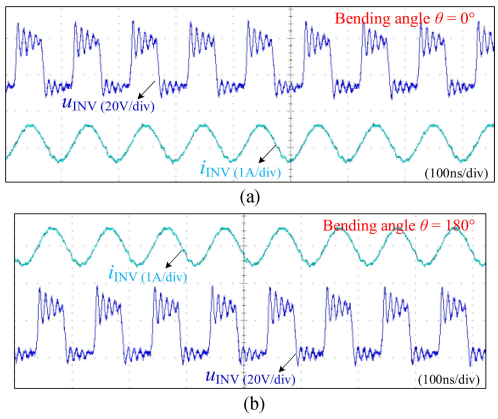

Fig. 14. Waveforms of u_{INV} and i_{INV}. (a) Bending angle is 0°. (b) Bending angle is 180°.

current and voltage are in the same phase, which can help the switches operate in soft-switching. Fig. 15 shows the output voltage V_{O}. The output voltage does not change significantly when the converter and aircore inductor are bent. The maximum deviation of the output voltage is about 25%. If the output voltage is expected to be limited in a narrow range, there must be a limitation for the bending angle. For the current research, the input impedance angle is taken as the main focus. In future work, a multiobjective optimization algorithm will be analyzed

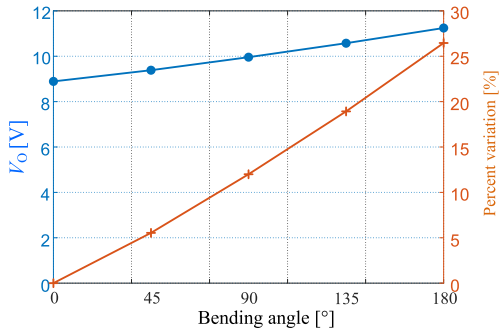

Fig. 15. Output voltage V_{O} of the prototype under different bending angles.

to further improve the performance of the proposed system and optimize the phase angle and output voltage at the same time.

In the soft switching state, the main losses of GaN-based inverter are capacitance loss and diode conduction loss of S_1 and S_2, which can be expressed as

$$P_C = \frac{1}{2} V_{\mathrm{in}}^2 C_{\mathrm{DS}} f_s \tag{15}$$

$$P_D = \frac{V_{S-D} I_{\mathrm{INV}}}{2\pi} \left[\cos\left(\pi - \varphi_{\mathrm{INV}}\right) - \cos\left(\omega t_2 - \varphi_{\mathrm{INV}}\right)\right] \tag{16}$$

where C_{DS} is the drain-source parasitic capacitor of the switch, $V_{\mathrm{S\text{-}D}}$ is the body diode conduction voltage, t_2 is the end time of capacitor charging, which can be calculated as

$$t_2 = \frac{\arccos\left[\frac{4\pi f C}{I_{\mathrm{INV}}}(V_{\mathrm{in}} + V_{S-D}) + \cos\left(2\pi D + \varphi_{\mathrm{INV}}\right)\right] - \varphi_{\mathrm{INV}}}{2\pi f}. \tag{17}$$

The main loss of the matching network comes from the coil resistance, which can be expressed as follows:

$$P_{\mathrm{coil}} = \frac{1}{2} \int \left(i_{\mathrm{REC}} - i_{\mathrm{INV}}\right)^2 R_{\mathrm{coil}} dt. \tag{18}$$

The loss of the rectifier is concentrated on the conduction loss of the diode, as shown in the following, where V_{D} is the forward conducting voltage of the diode:

$$P_D = V_D I_O. \tag{19}$$

The calculated loss of each component under different bending angles is shown in Fig. 16. Since the proposed topology can suppress the change of impedance angle, the loss of the inverter $P_{\mathrm{S1}} + P_{\mathrm{S2}}$ remains relatively stable when the coil is bent. On the other hand, inductance loss $P_{\mathrm{L\text{-}bent}}$ and diode loss $P_{\mathrm{D1}} + P_{\mathrm{D2}}$ increase with bending, this is because the decrement of coil inductance caused during the bending will further increase the matching network gain G (u_{REC} / u_{INV}), resulting in an increment of coil current i_{coil}.

The efficiency under different bending angles is shown in Fig. 17. Compared with the conventional design method, the overall efficiency of the system is higher and more stable because of the maintenance of resistive input impedance and soft-switching.

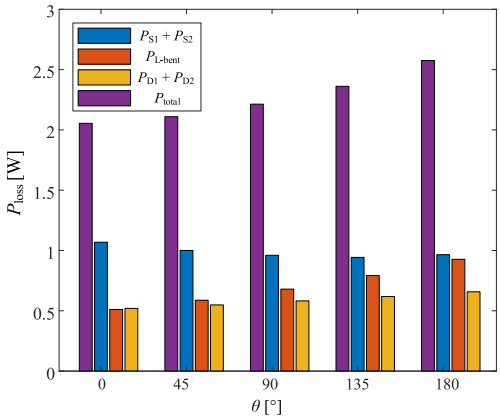

Fig. 16. Calculated loss of the prototype under different bending angles.

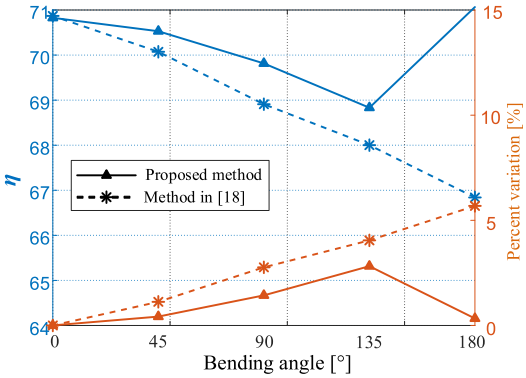

Fig. 17. Efficiency comparison under different bending angles.

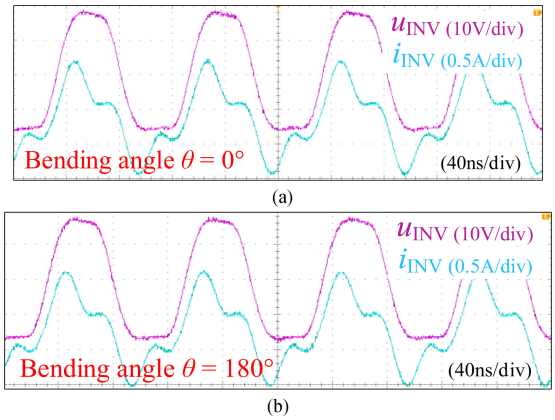

Fig. 18. Voltage and current waveforms with Coil 1. (a) Bending angle is 0°. (b) Bending angle is 180°.

When the shape of the coil changes, it can also be analyzed based on the proposed process: first derive the space coordinates, then find the self-inductance and mutual inductance by integral operation, finally, the inductance value can also be solved. Based on the calculation results of the bendable coil in Fig. 3, experiments have been carried out with different coils, and the relevant waveforms are shown in Figs. 18–21. It can be seen

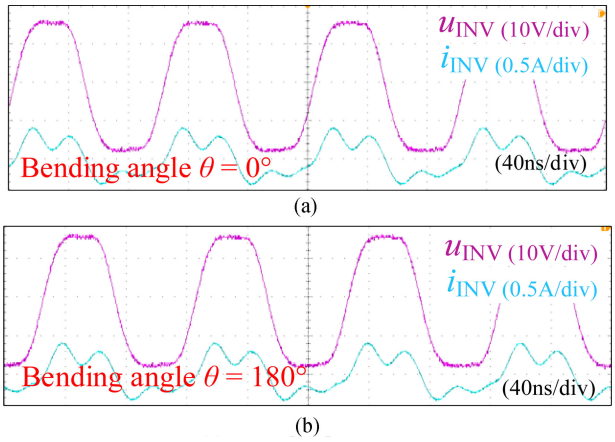

Fig. 19. Voltage and current waveforms with Coil 2. (a) Bending angle is 0°. (b) Bending angle is 180°.

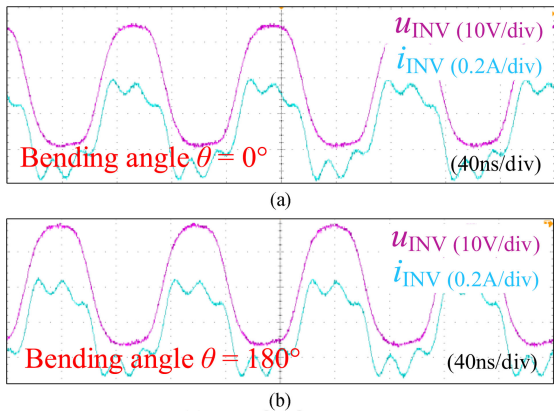

Fig. 20. Voltage and current waveforms with Coil 3. (a) Bending angle is 0°. (b) Bending angle is 180°.

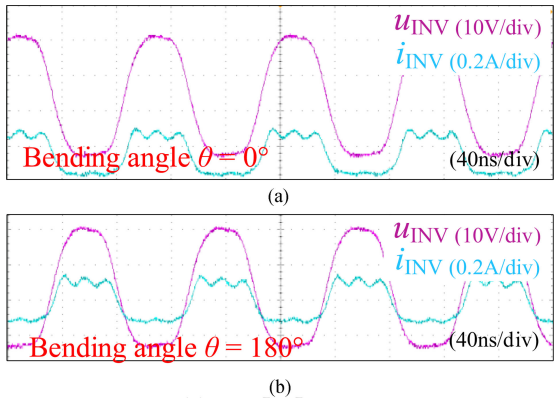

Fig. 21. Voltage and current waveforms with Coil 4. (a) Bending angle is 0°. (b) Bending angle is 180°.

that the impedance angle remains the same under 0° and 180° bending angles.

In addition, the design of the topology also can be applied to any bendable aircore inductor. Under other topologies, by

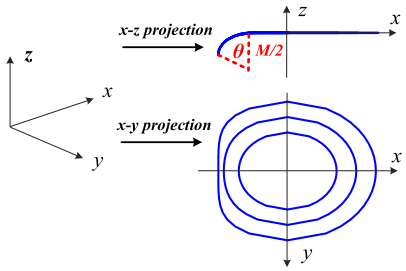

Fig. 22. Space projection of noncentrosymmetric bent coil.

substituting different objective functions, the topology can also be designed for the condition of inductance variation.

V. Conclusion

This article proposes an optimal design method of T type matching network of a 10 MHz bendable dc/dc converter with planar aircore coil. In this article, the mathematical calculation method of the bendable planar circular coil is analyzed, and the accuracy of the inductance calculation is verified. The T-matching network is optimally designed to maintain expected input impedance characteristics considering the variable inductance effect. A 10 MHz, 9 V/6.3 W with 32 V input voltage prototype is built to verify the feasibility of the proposed design method, which owns higher efficiency under bending situations.

Appendix

When the coil is bent asymmetrically, the projection diagram of the coil on *xy* and *yz* planes is shown in Fig. 22. A general situation is given where the left side of the coil is bent with a radius of $M/2$ and an angle of θ, while the right side keeps its original shape. For any other bending situations, it can be analyzed with a similar method.

Similar to the analysis in Section II, by taking the coil coordinates and the partial conductance into (4), and then through the program subsection summation, the coil inductance values under different angles and radius can be obtained, where the coordinates of different parts of the coil can be obtained as (20) as shown at bottom of this page.

References

[1] G. Martínez, J. M. Alonso, and R. O. Sánchez, "Simplified photo-electro-thermal model applied to resonant-switched-capacitor-based OLED drivers," in *Proc. IEEE Ind. Appl. Soc. Annu. Meeting*, 2019, pp. 1–8.

[2] J. Hu, "Overview of flexible electronics from ITRI's viewpoint," in *Proc. 28th VLSI Test Symp.*, 2010, pp. 84–84.

[3] B. M. Kayes, L. Zhang, R. Twist, I. Ding, and G. S. Higashi, "Flexible thin-film tandem solar cells with >30% efficiency," *IEEE J. Photovolt.*, vol. 4, no. 2, pp. 729–733, Mar. 2014.

[4] M. Tian, X. Yang, Y. Chen, W. Chen, and L. Wang, "Design, modeling, and optimization of a coaxial cable-embedded flexible inductor for wearable applications," *IEEE J. Emerg. Sel. Topics Power Electron.*, vol. 7, no. 3, pp. 1691–1702, Sept. 2019.

[5] Y. Wang, W. Liu, and Y. Xie, "Design and optimization for circular planar spiral coils in wireless power transfer system," in *Proc. 22nd Int. Conf. Elect. Mach. Syst.*, 2019, pp. 1–4.

[6] S. S. Mohan, M. del Mar Hershenson, S. P. Boyd, and T. H. Lee, "Simple accurate expressions for planar spiral inductances," *IEEE J. Solid-State Circuits*, vol. 34, no. 10, pp. 1419–1424, Oct. 1999.

[7] H. Greenhouse, "Design of planar rectangular microelectronic inductors," *IEEE Trans. Parts , Hybrids, Packag.*, vol. 10, no. 2, pp. 101–109, Jun. 1974.

[8] M. Tian *et al.*, "A wire-embedded converter used for wearable devices," *Proc. IEEE Appl. Power Electron. Conf. Expo.*, 2017, pp. 121–125.

[9] Y. Fang and M. H. Pong, "A Bayesian optimization and partial element equivalent circuit approach to coil design in inductive power transfer systems," in *Proc. IEEE PELS Workshop Emerg. Technol., Wireless Power Transfer*, 2018, pp. 1–5.

[10] G. K. Y. Ho, B. M. H. Pong, and R. S. Y. Hui, "LLC resonant converter design for bendable power converter," in *Proc. IEEE Appl. Power Electron. Conf. Expo.*, 2016, pp. 2328–2333.

[11] S. Jeong *et al.*, "Smartwatch strap wireless power transfer system with flexible PCB coil and shielding material," *IEEE Trans. Ind. Electron.*, vol. 66, no. 5, pp. 4054–4064, May 2019.

[12] K. Aikawa, H. Sato, and M. Uno, "Bendable differential power processing converter for curved photovoltaic panels," *in Proc. 10th Int. Conf. Power Electron. ECCE Asia*, 2019, pp. 1–7.

[13] G. K. Y. Ho, Y. Fang, and B. M. H. Pong, "A multiphysics design and optimization method for air-core planar transformers in high-frequency LLC resonant converters," *IEEE Trans. Ind. Electron.*, vol. 67, no. 2, pp. 1605–1614, Feb. 2020.

[14] N. B. Narampanawe, K. Y. See, J. Zhang, E. K. Chua, and W. P. Goh, "Analysis of ultra-thin and flexible current transformer based on JA hysteresis model," *IEEE Sensors J.*, vol. 17, no. 13, pp. 4029–4036, Jan. 2017.

[15] G. K. Y. Ho, C. Zhang, B. M. H. Pong, and S. Y. R. Hui, "Modeling and analysis of the bendable transformer," *IEEE Trans. Power Electron.*, vol. 31, no. 9, pp. 6450–6460, Sept. 2016.

[16] R. Sinha and A. De, "Theory on matching network in viewpoint of transmission phase shift," *IEEE Trans. Microw. Theory Techn.*, vol. 64, no. 6, pp. 1704–1716, Jun. 2016.

[17] R. Erickson and D. Maksimovic, *Fundamentals of Power Electronics*, 2nd ed. New York, NY, USA: Springer Science+Business, 2001.

[18] Y. Guan *et al.*, "Analysis and design of high-frequency converter with resistive matching network and spiral inductor," *IEEE Trans. Power Electron.*, vol. 33, no. 6, pp. 5062–5075, Jun. 2018.

[19] Y. Guan, C. Liu, Y. Wang, W. Wang, and D. Xu., "Analytical derivation and design of 20-MHz DC–DC soft-switching resonant converter," *IEEE Trans. Ind. Electron.*, vol. 68, no. 1, pp. 210–221, Jan. 2021.

[20] M. Liu, S. Liu, and C. Ma, "A high-efficiency/output power and low-noise megahertz wireless power transfer system over a wide range of mutual inductance," *IEEE Trans. Microw. Theory Techn.*, vol. 65, no. 11, pp. 4317–4325, Nov. 2017.

[21] K. Zhang, W. Gao, R. Shi, Z. Yan, B. Song, and A. P. Hu, "An impedance matching network tuning method for constant current output under mutual inductance and load variation of IPT system," *IEEE Trans. Power Electron.*, vol. 35, no. 10, pp. 11108–11118, Oct. 2020.

[22] Y. Lim, H. Tang, S. Lim, and J. Park, "An adaptive impedance-matching network based on a novel capacitor matrix for wireless power transfer," *IEEE Trans. Power Electron.*, vol. 29, no. 8, pp. 4403–4413, Aug. 2014.

$$
\begin{cases}
i_+(x,y,z) = \left[\sqrt{r_i^2-y^2}, y, 0\right] & y \in [-B_i, B_i] \\
i_-(x,y,z) = \begin{cases}
\left[-\sqrt{r_i^2-y^2}, y, 0\right] & y \in [-r_i, -y_{\lim}], [y_{\lim}, r_i] \\
\left[-\frac{M}{2}\sin\left(\frac{2\sqrt{r_i^2-y^2}-2R_N-M\theta}{M}\right)+\frac{M\theta}{2}-R_N,\right. & \\
\left. y, \frac{M}{2}\cos\left(\frac{2\sqrt{r_i^2-y^2}-2R_N-M\theta}{M}\right)-\frac{M}{2}\right] & y \in [-y_{\lim}, y_{\lim}]
\end{cases}
\end{cases}
\tag{20}
$$

[23] C. Liu, Y. Guan, Y. Wang, W. Wang, and D. Xu, "Design of matching network in high frequency converter considering flexible aircore inductor effect," in *Proc. IEEE 21st Workshop Control Model Power Electron.*, 2020, pp. 1–6.
[24] Y. Lim, H. Tang, S. Lim, and J. Park, "An adaptive impedance-matching network based on a novel capacitor matrix for wireless power transfer," *IEEE Trans. Power Electron.*, vol. 29, no. 8, pp. 4403–4413, Aug. 2014.
[25] J. Li, V. F. Tseng, Z. Xiao, and H. Xie, "A high-Q in-silicon power inductor designed for wafer-level integration of compact DC–DC converters," *IEEE Trans. Power Electron.*, vol. 32, no. 5, pp. 3858–3867, May 2017.
[26] D. Hou, F. C. Lee, and Q. Li, "Very high frequency IVR for small portable electronics with high-current multiphase 3-D integrated magnetics," *IEEE Trans. Power Electron.*, vol. 32, no. 11, pp. 8705–8717, Nov. 2017.

Yueshi Guan (Member, IEEE) was born in Heilongjiang Province, China, in 1990. He received the B.S., M.S., and Ph.D. degrees in electrical engineering from Harbin Institute of Technology (HIT), Harbin, China, in 2013, 2015 and 2019, respectively.

Since 2019, he has been an Associate Professor with the Department of Electrical and Electronics Engineering, HIT. His research interests include the areas of high frequency and very high frequency converters, single-stage ac/dc converter, and high conversion ratio converters.

Chang Liu (Student Member, IEEE) was born in Jilin Province, China, in 1997. She received the B.S. degree in electrical engineering in 2019 from Harbin Institute of Technology, Harbin, China, where she is currently working toward the M.S. degree in electrical engineering.

Her current research interests include high-frequency and very-high-frequency converters.

Yijie Wang (Senior Member, IEEE) was born in Heilongjiang Province, China, in 1982. He received the B.S., M.S., and Ph.D. degrees in electrical engineering from Harbin Institute of Technology, Harbin, China, in 2005, 2007, and 2012, respectively.

From 2012 to 2014, he was a Lecturer with the Department of Electrical and Electronics Engineering, Harbin Institute of Technology. Since 2015, he has been an Associate Professor with the Department of Electrical and Electronics Engineering, Harbin Institute of Technology. His interests include dc–dc converters, soft-switching power converters, power factor correction circuits, digital control electronic ballasts, and LED lighting systems.

Wei Wang was born in Heilongjiang Province, China, in 1963. She received the B.S. degrees in automatic test and control, the M.S. degree in electrical engineering, and the PH.D. degree in mechanical electronic engineering from Harbin Institute of Technology, Harbin, China, in 1984, 1990 and 2002, respectively.

Since 2003, she has been a Professor with the Department of Electrical Engineering, Harbin Institute of Technology. Her research interests include soft-switching converters, digital control electronic ballast, and regenerative energy converter technique.

Dianguo Xu (Fellow, IEEE) was born in Heilongjiang, China, in 1960. He received the B.S. degree in control engineering from Harbin Engineering University, Harbin, China, in 1982, and the M.S. and Ph.D. degrees in electrical engineering from Harbin Institute of Technology (HIT), Harbin, China, in 1984 and 1989, respectively.

In 1984, he joined the Department of Electrical Engineering, HIT, as an Assistant Professor and has been a Professor since 1994. From 2000 to 2010, he was the Dean of School of Electrical Engineering and Automation, HIT. He is currently the Vice President of HIT. He has authored or coauthored more than 600 technical papers. His research interests include renewable energy generation technology, power quality mitigation, sensorless vector controlled motor drives, and high performance servo system.

Dr. Xu is a fellow of IEEE, an Associate Editor of the IEEE TRANSACTIONS ON INDUSTRIAL ELECTRONICS and the IEEE JOURNAL OF EMERGING AND SELECTED TOPICS IN POWER ELECTRONICS. He serves as Chairman of IEEE Harbin Section.